AN ORIGINAL PROBE OF DARK MATTER IN THE CORE OF M87 WITH THE EVENT HORIZON TELESCOPE

T. LACROIX

Laboratoire Univers & Particules de Montpellier (LUPM), CNRS & Université de Montpellier (UMR 5299), Place Eugène Bataillon, F-34095 Montpellier Cedex 05, France

Institut d'Astrophysique de Paris, UMR 7095, CNRS, UPMC Université Paris 6, Sorbonne Universités, 98 bis boulevard Arago, 75014 Paris, France

We demonstrate the unprecedented capabilities of the Event Horizon Telescope (EHT) to image the innermost dark matter profile in the vicinity of the supermassive black hole at the center of the M87 radio galaxy. We present the first model of the synchrotron emission induced by dark matter annihilations from a spiky profile in the close vicinity of a supermassive black hole, accounting for strong gravitational lensing effects. Our results show that the EHT should readily resolve dark matter spikes if present. Moreover, the photon ring surrounding the silhouette of the black hole is clearly visible in the spike emission, which introduces observable small-scale structure into the signal. We find that the dark matter-induced emission provides an adequate fit to the existing EHT data, implying that in addition to the jet, a dark matter spike may account for a sizable portion of the millimeter emission from the innermost (sub-parsec) region of M87. Regardless, our results show that the EHT can probe very weakly annihilating dark matter. Current EHT observations already constrain very small cross-sections, typically down to a few 10^{-31} cm^3 s^{-1} for a 10 GeV candidate. Future EHT observations will further improve constraints on the DM scenario.

1 Introduction

The central regions of galaxies are of particular interest for the astrophysical community as the sites of very diverse high-energy processes, including putative annihilation of dark matter (DM) particles. In this context, the DM energy density profile at the centers of galaxies is critical for indirect searches but remains poorly constrained. In objects such as the M87 giant radio galaxy, the DM profile may be significantly enhanced on sub-parsec scales by the central supermassive black hole (SMBH), although there is no direct evidence yet for such a sharp density increase, referred to as a DM spike.

Here we show that it is possible to probe very faint DM-induced radiation in the very inner region of M87 by using the spatial morphology of the DM-induced synchrotron emission near the central black hole (BH). Due to a lack of angular resolution in existing observational facilities, such a study of the DM-induced signal in the inner part of M87 has not been performed yet—nor has it been done in similar objects. However, this is now possible with the advent of the Event Horizon Telescope (EHT),[a] for which the M87 galaxy is a prime target.

[a] http://www.eventhorizontelescope.org/

2 Dark matter spikes at the centers of galaxies?

The DM energy density profile $\rho(r)$ in galaxies is very uncertain, especially below parsec scales, where it can be significantly affected by the presence of a central SMBH. In particular, the scenario of adiabatic growth of a SMBH at the center of a DM halo with power-law density profile should lead to a strong enhancement of the DM density, referred to as a spike, and corresponding to $\rho(r) \propto r^{-\gamma_{\rm sp}}$ with typically $\gamma_{\rm sp} = 7/3$ on sub-pc scales [1].

However, such a strong morphological feature can be subsequently affected by galactic dynamics. On the one hand, it can be weakened by various dynamical processes such as mergers [2] (although the resolution of numerical simulations used to reach that conclusion is not sufficient to set strong constraints on the profile on sub-pc scales), if the BH did not grow close enough to the center of the DM halo [3,4], or if the BH growth occurred to fast to be considered adiabatic [4]. Moreover, dynamical heating in the central stellar core would also soften a spike. However, an adiabatic spike is more likely to have survived in a dynamically young galaxy such as M87, in which stellar heating is essentially negligible [5,6]. On the other hand, other dynamical processes can have the opposite effect of making the formation and survival of a steep spike more likely; for instance enhanced accretion of DM to counteract the depopulation of chaotic orbits in triaxial halos [7]. As a result, the picture is unclear at present, and this scenario needs to be tested with dedicated probes.

Therefore, in the following we consider the scenario in which an adiabatic spike effectively formed at early times at the center of M87 and has survived until today. We study the observability of such a feature, in the context of the observational opportunities offered by the EHT, and taking advantage of the strong DM annihilation signals expected.

3 The Event Horizon Telescope

3.1 General features

The EHT is a global network of millimeter and submillimeter facilities that employs very long baseline interferometry (VLBI) to create an effective Earth-scale high angular resolution telescope [8,9]. The purpose of this array is to test general relativity and shed light on physical processes taking place in the vicinity of SMBHs at the centers of galaxies. To date, EHT data for M87 has been reported for a 3-station array comprised of the Submillimeter Telescope (SMT) in Arizona, the Combined Array for Research in Millimeter-wave Astronomy (CARMA) in California, and a network of three facilities in Hawaii: the James Clerk Maxwell Telescope (JCMT), the Submillimeter Array (SMA), and the Caltech Submillimeter Observatory (CSO). This configuration has already achieved an impressive angular resolution of order 40 μas at 230 GHz. Presently, the Atacama Large Millimeter/submillimeter Array (ALMA) in Chile, the Large Millimeter Telescope (LMT) in Mexico, the Institut de Radioastronomie Millimétrique (IRAM) 30m, the Plateau de Bure interferometer, and the South Pole Telescope (SPT)[b] will be added to the EHT. Longer term, the Greenland Telescope will join the array. Combined, the EHT will directly access angular scales as small as 26 μas at 230 GHz and 17 μas at 345 GHz.

The angular scale of the Schwarzschild radius of the SMBH at the center of M87 is about 8 μas.[c] The strong gravitational lensing near the black hole (BH) magnifies this by a factor of as much as 2.5, only weakly dependent of BH spin, making M87 a primary target for the EHT [9].

[b] Note that M87 cannot be seen by the SPT.

[c] The mass of the central BH is $M_{\rm BH} = (6.4 \pm 0.5) \times 10^9 M_\odot$ [10], the corresponding Schwarzschild radius is $R_{\rm S} = 6 \times 10^{-4}$ pc and the distance of M87 is $d_{\rm M87} \approx 16$ Mpc [11]. Throughout we adopt the higher stellar dynamical mass for M87; using the $(3.5 \pm 0.8) \times 10^9 M_\odot$ value found by gas dynamical studies [12] would reduce the angular scales by roughly a factor of two throughout.

3.2 Imaging the shadow of a black hole

Characteristic in all images of optically thin emission surrounding BHs is a "shadow"—a dark central region surrounded by a brightened ring, the so-called "photon ring". This is a direct consequence of the strong gravitational lensing near the photon orbit, and is directly related to the projected image of the photon orbit at infinity. The shadow interior is the locus of null geodesics that intersect the horizon, and thus does not contain emission from behind the BH. The bright ring is in general sharply defined due to the instability of the photon orbit and a consequence of the pileup of higher-order images of the surrounding emission. For a Schwarzschild BH the radius of this shadow is $r_{\rm shadow} = 3\sqrt{3}/2R_{\rm S} \approx 2.6R_{\rm S}$ [13,14]. For Kerr BHs, this radius ranges from $2.25R_{\rm S}$ to $2.6R_{\rm S}$, deviating substantially only at large values of the dimensionless spin parameter a and viewed from near the equatorial plane, i.e., $a > 0.9$ and $\theta > 60^\circ$ [15].

The generic appearance of the shadow, its weak dependence on BH spin, and fundamentally general relativistic origin make it a prime feature in EHT science. Also imprinted on EHT images will be the high-energy astrophysics of the near-horizon region; the physics of BH accretion and relativistic jet formation. In this work, we assess the observability of the shadow of the SMBH at the center of M87 in the electromagnetic signal from DM annihilation, and the limits that may be placed on DM properties given such a scenario.

4 Probing DM at the center of M87 with the EHT

At the frequencies of interest for the EHT, typically a few hundred GHz, the main DM signature comes from synchrotron radiation. Therefore, in order to assess the ability of the EHT to probe the inner part of the DM profile of M87, we compute the intensity of the synchrotron emission of electrons and positrons produced in DM annihilations in the inner region. To this end, we first need to compute the electron and positron spectra from the DM annihilation rate which is proportional to the thermally averaged cross section $\langle \sigma v \rangle$ and the square of the DM density. This is done by solving the propagation equation of DM-induced electrons and positrons in the presence of synchrotron radiation and advection towards the central BH. This procedure is described in detail in the associated paper [16]. We assume the intensity of the magnetic field to be homogeneous in the region of interest. The spatial morphology of the synchrotron intensity I_ν is obtained using a dedicated ray-tracing and radiative transfer scheme that accounts for the gravitational lensing effect due to the BH [17,18,19].

4.1 Interferometric observables and data used in this work

Here we provide a brief overview of the EHT data used to constrain our models. The EHT, like all interferometers, directly constructs visibilities by cross-correlating observations at pairs of stations. These are directly proportional to the Fourier transform of the image at a spatial frequency proportional to the ratio of the projected baseline distance between the two stations to the observation wavelength. Throughout the night the rotation of the Earth results in a rotation of the projected baseline, changing both its orientation and length, thereby generating a moderate variation in the spatial frequencies probed by any particular pair of sites.

Upon measuring a sufficient number of these visibilities an image can be produced via inverting the Fourier transform. However, because the published EHT observations only sparsely sample the spatial-frequency plane (often called the "u-v" plane) we compare directly with the measured visibilities.

By construction the visibilities are complex valued, and therefore described by an amplitude and phase. However, in practice the amplitudes are known much better than the phases as a result of the typically large, and highly variable, atmospheric phase delays. This does not mean that phase information is completely unavailable; "closure phases" constructed from triplets of

sites, equal to the sum of the phases over the closed triangle of baselines, are insensitive to site-specific phase errors. Therefore, the two data sets we employ consist of visibility amplitudes and closure phases obtained with the Hawaii-SMT-CARMA array [20,21]. In all cases observations were taken at 230 GHz.

On the Hawaii-CARMA-SMT triangle, 17 closure phases were constructed from data taken on March 21, 2012 [21]. Where visibility amplitudes provide a measure of the "power" in an image at a given spatial scale, closure phases are particularly sensitive to asymmetry; e.g., a point-symmetric image has identically zero closure phases. These are consistent with a constant closure phase of 0°, with typical uncertainties of 10°.

4.2 Results

Intensity maps

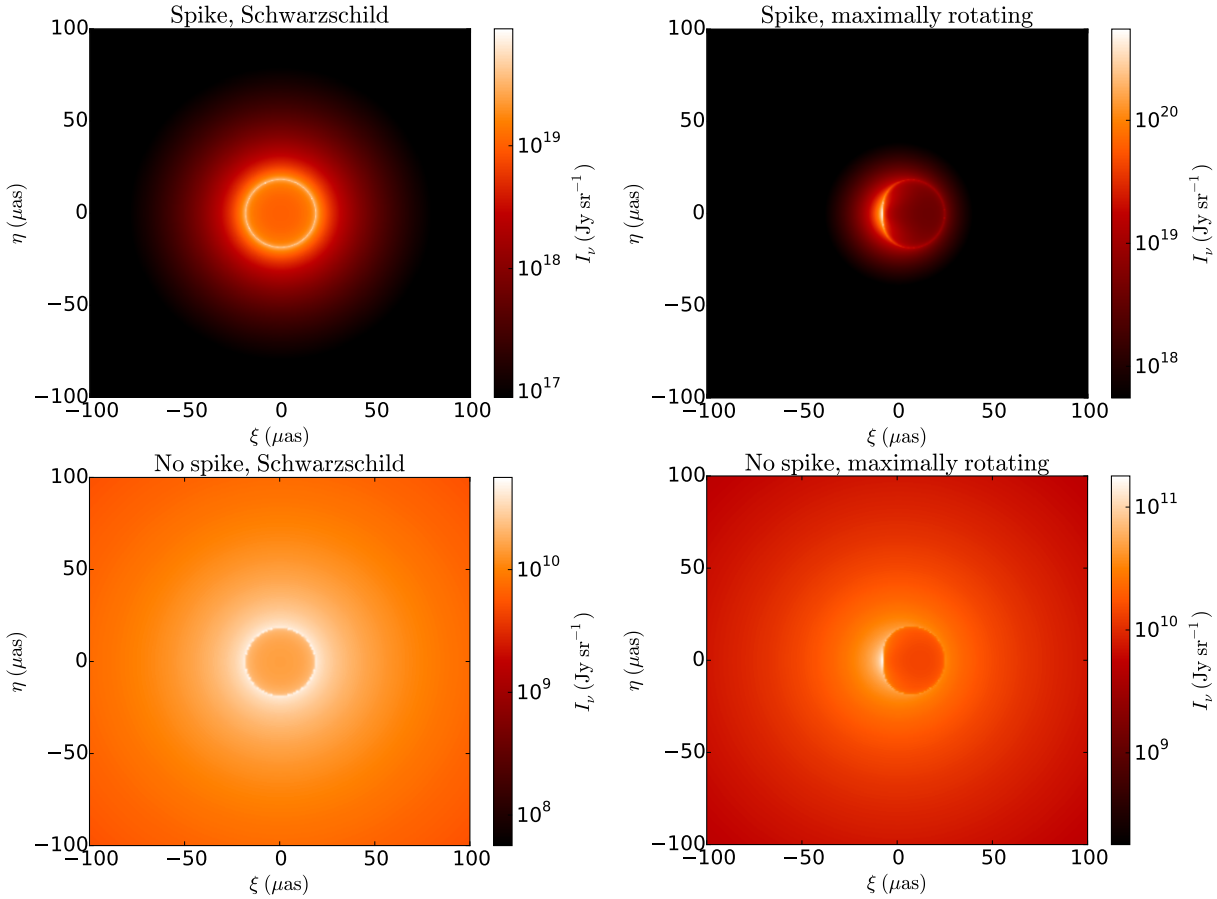

Figure 1 – Simulated maps of the synchrotron intensity at 230 GHz from a spike of 10 GeV DM annihilating into $b\bar{b}$, accounting for the strong gravitational lensing induced by the central BH, for a Schwarzschild BH (left panel) and a maximally rotating BH (right panel), in the presence (upper panels) and absence (lower panels) of a spike in the DM profile. Note that considering the wide range of intensities, we use different color scales, but with the same dynamic range spanning three orders of magnitude for comparison. The angular coordinates ξ and η correspond to the directions respectively perpendicular and parallel to the spin of the BH. For the spike cases, the slope of the DM spike is $\gamma_{\rm sp} = 7/3$, and the annihilation cross-sections correspond to the best fit to EHT observations, namely 7.4×10^{-31} cm^3 s^{-1} for the Schwarzschild case and 3.1×10^{-31} cm^3 s^{-1} for the maximally rotating case. In the absence of a spike, the intensity is computed for the thermal s-wave cross-section of 3×10^{-26} cm^3 s^{-1}. For all the simulated maps the magnetic field is 10 G.

Predicted images are shown in Fig. 1, corresponding to the synchrotron intensity at 230 GHz from DM [16]. The upper panels correspond to a DM spike with $\gamma_{\rm sp} = 7/3$, whereas the maps in the lower panels are computed for the no-spike case, for which we consider a standard

Navarro-Frenk-White (NFW) DM profile with power-law index $\gamma = 1$. We assume annihilation of 10 GeV DM particles into $b\bar{b}$,[d] and a magnetic field of 10 G, for a static BH (left panels) and a maximally rotating BH (right panels).

The photon ring, i.e. the bright ring of radius ~ 20 μas that surrounds the darker shadow of the BH, is clearly visible in the simulations for all DM models we consider, although in practice in the absence of a spike the signal is too weak to be detectable with the EHT, as discussed in the following. The presence of a photon ring introduces small-scale structure into the signal, readily observable with the EHT on long baselines. For a static BH the shadow is exactly circular. For all but the most rapidly rotating BHs it is also very nearly circular [22,23]. For a maximally rotating Kerr BH viewed from the equatorial plane the photon ring is flattened in the direction aligned with the BH spin.

Fig. 1 also illustrates the fact that the intensity is significantly enhanced in the presence of a DM spike with respect to the no-spike case. To better stress this enhancement, we show the maps for the spike case computed for very small annihilation cross-sections of a few 10^{-31} cm^3 s^{-1}—corresponding to the best fits to the EHT data, as discussed below—, while in the absence of a spike we use the thermal s-wave cross-section of 3×10^{-26} cm^3 s^{-1}. In addition, the contrast on the photon ring is also enhanced in the presence of a DM spike.

Visibility amplitudes

Shown in the blue solid line in Fig. 2 is the visibility amplitude at 230 GHz as a function of baseline length for the current EHT triangle, for the simulated DM-induced synchrotron signal, computed with a cross-section that gives the best fit to the EHT measurements [16]. The left panel corresponds to the Schwarzschild case and the right panel to the maximally rotating case. The DM-induced visibility amplitudes shown in Fig. 2 correspond to the intensity maps shown in Fig. 1. Note that no additional astrophysical component has been included in these. A standard NFW cusp actually results in visibility amplitudes that are about eight orders of magnitude lower than the EHT data. Note that these no-spike visibility amplitudes are not shown in Fig. 2 for clarity. Therefore, the EHT is only sensitive to spiky profiles, which makes it a dedicated probe of such sharply peaked DM distributions.

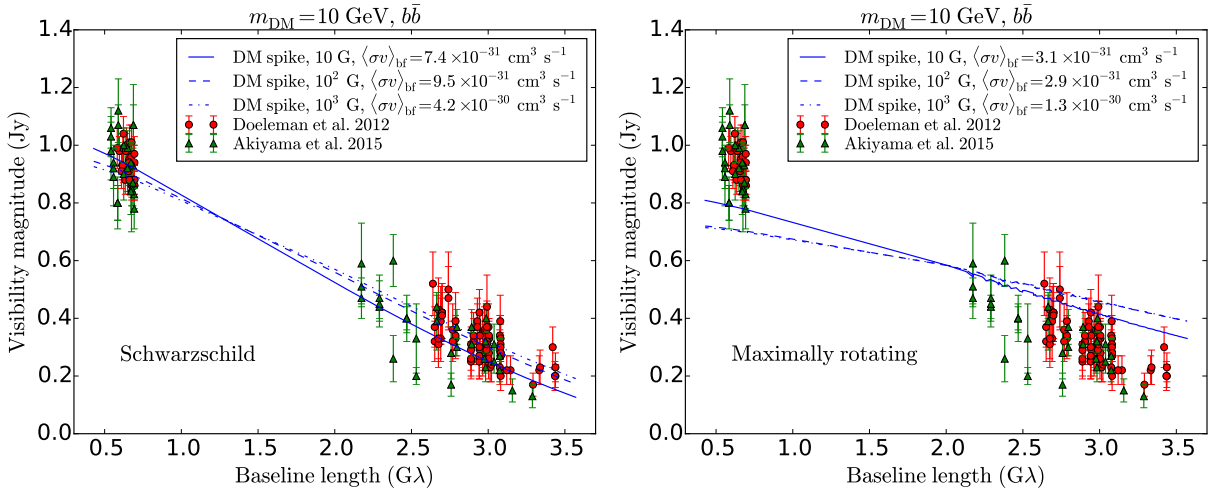

Figure 2 – Visibility amplitude at 230 GHz as a function of baseline length. The blue solid line represents the synchrotron emission from a spike of 10 GeV DM annihilating into $b\bar{b}$, with $B = 10$ G (solid), $B = 10^2$ G (dashed), and $B = 10^3$ G (dot-dashed), for a Schwarzschild BH (left panel) and a maximally rotating BH (right panel). The annihilation cross-sections correspond to the best fit to the EHT data [20,21].

[d] We focus on the standard b quark channel for simplicity. Injection of electrons through a different channel would primarily result in a rescaling of the intensity at the frequency of interest, slightly changing the best fit cross-sections we derive.

As shown in Fig. 2, a spike of annihilating DM gives a good fit to the EHT measurements of the visibility amplitudes, with best fit cross-sections of 7.4×10^{-31} cm^3 s^{-1} for the Schwarzschild case and 3.1×10^{-31} cm^3 s^{-1} for the maximally rotating case. While the fits appear by eye to be quite good, the reduced chi-squareds coupled with the large number of degrees of freedom result in a p-value < 0.002, implying that some structural component is missing in our model. This is not, in itself, surprising given the extraordinary simplicity of the DM spike model and our neglect of the contributions from the observed larger-scale radio emission associated with the jet.

We note that the morphology of the predicted visibility amplitudes is only weakly sensitive to changes in the DM mass, the annihilation channel or the magnetic field, resulting primarily in different best-fit cross-sections, as shown in the dashed and dot-dashed lines in Fig. 2.

Closure phases

The closure phases for the DM-spike-induced signal are shown in Fig. 3, for the Schwarzschild case (solid line) and the maximally rotating case (dashed line) [16]. The symmetry of the simulated signal is insensitive to the various parameters so we do not need to specify them here. As expected, the closure phase is identically zero for a Schwarzschild BH, while it is slightly larger than zero for the maximally rotating case. In both cases, closure phases for the DM-induced emission are consistent with the low closure phases observed.

Small closure phases are also typical of astrophysical models on the Hawaii-CARMA-SMT triangle [21]. This is because of the near degenerate nature of the projected baseline triangle due to the comparatively short CARMA-SMT baseline; closure phases on trivial triangles (in which one baseline has zero length) vanish identically. However, the inclusion of a number of additional sites in the near future will result in many additional, open triangles for which the closure phases are likely to differ substantially from zero [21]. These will be instrumental to discriminating both between astrophysical and DM-dominated models.

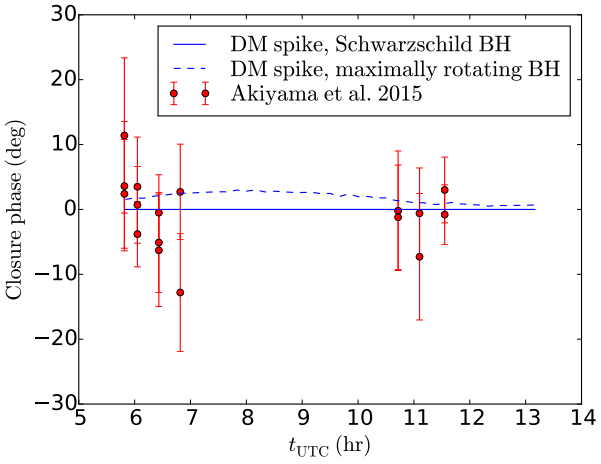

Figure 3 – Closure phase as a function of universal time, for a Schwarzschild BH (solid) and a maximally rotating BH (dashed), for the current VLBI triangle between Arizona, California and Hawaii.

5 Conclusion

In this work, we have demonstrated the potential of the EHT for DM searches. We have presented the first model of the DM-induced synchrotron emission in the close vicinity of a SMBH accounting for strong gravitational lensing effects.

The synchrotron emission from DM spikes should be readily visible in EHT images of M87 if present. This remains true even for very small values of the annihilation cross-section. The re-

sulting emission follows the structure of the DM spike, resulting in a synchrotron halo extending from horizon scales to roughly 100 μas.

Within the spike emission, the silhouette of the BH is clearly visible on small scales for all spins and models we considered. This imparts small-scale structure on the image on scales of 50 μas, and contributes substantially to the visibilities on long baselines.

DM spike emission provides an adequate fit to the existing horizon-scale structural constraints from the EHT. This necessarily ignores astrophysical contributions associated with the jet launching region. Such an additional astrophysical component is strongly motivated by the existence of extended emission at wavelengths of 3 mm and longer. Even within the 1.3 mm data, the fit quality suggests that the simple spike structures we present here are incomplete.

Nevertheless, the limits on M87's flux and small-scale structure place corresponding constraints on the putative DM annihilation cross-sections. For a 10 GeV DM candidate this cross-section must be less than a few 10^{-31} cm^3 s^{-1}, close to the characteristic cross-sections for p-wave-suppressed annihilation. The introduction of additional astrophysical components would decrease this limit further.

EHT observations in the near future will include a number of additional stations, enabling the reconstruction of M87's image with substantially higher fidelity. As a result, the limits on the existence of DM spikes and the properties of DM candidates will similarly improve. Thus, the EHT opens a new, powerful path to probing the structure and features of DM in the centers of galaxies.

Acknowledgments

This project has been completed in collaboration with Mansour Karami, Avery E. Broderick, Joseph Silk and Céline Bœhm. This work has been supported by UPMC, CNRS and STFC. This research has also received support at IAP from the ERC Project No. 267117 (DARK) hosted by UPMC, and has been carried out in the ILP LABEX (ANR-10-LABX-63) and supported by French state funds managed by the ANR, within the Investissements d'Avenir programme (ANR-11-IDEX-0004-02). A.E.B. and M.K. receive financial support from the Perimeter Institute for Theoretical Physics and the Natural Sciences and Engineering Research Council of Canada through a Discovery Grant. Research at Perimeter Institute is supported by the Government of Canada through Industry Canada and by the Province of Ontario through the Ministry of Research and Innovation. We acknowledge support by the Canadian Institute for Advanced Research for the participation of A.E.B. and J.S. at the annual meetings of the CIFAR cosmology program where this project was initiated.

References

1. P. Gondolo and J. Silk. Dark Matter Annihilation at the Galactic Center. *Phys. Rev. Lett.*, 83:1719–1722, August 1999.
2. D. Merritt, M. Milosavljević, L. Verde, and R. Jimenez. Dark Matter Spikes and Annihilation Radiation from the Galactic Center. *Physical Review Letters*, 88(19):191301, May 2002.
3. T. Nakano and J. Makino. On the Cusp around Central Black Holes in Luminous Elliptical Galaxies. *ApJL*, 525:L77–L80, November 1999.
4. P. Ullio, H. Zhao, and M. Kamionkowski. Dark-matter spike at the galactic center? *Phys. Rev. D*, 64(4):043504, August 2001.
5. E. Vasiliev and M. Zelnikov. Dark matter dynamics in the galactic center. *Phys. Rev. D*, 78(8):083506, October 2008.
6. T. Lacroix, C. Bœhm, and J. Silk. Ruling out thermal dark matter with a black hole induced spiky profile in the M87 galaxy. *Phys. Rev. D*, 92(4):043510, August 2015.

7. D. Merritt and M. Y. Poon. Chaotic Loss Cones and Black Hole Fueling. *ApJ*, 606:788–798, May 2004.
8. S. Doeleman. Building an event horizon telescope: (sub)mm VLBI in the ALMA era. In *10th European VLBI Network Symposium and EVN Users Meeting: VLBI and the New Generation of Radio Arrays*, page 53, 2010.
9. R.-S. Lu, A. E. Broderick, F. Baron, et al. Imaging the Supermassive Black Hole Shadow and Jet Base of M87 with the Event Horizon Telescope. *ApJ*, 788:120, June 2014.
10. K. Gebhardt and J. Thomas. The Black Hole Mass, Stellar Mass-to-Light Ratio, and Dark Halo in M87. *ApJ*, 700:1690–1701, August 2009.
11. S. Bird, W. E. Harris, J. P. Blakeslee, and C. Flynn. The inner halo of M 87: a first direct view of the red-giant population. *A&A*, 524:A71, December 2010.
12. J. L. Walsh, A. J. Barth, L. C. Ho, and M. Sarzi. The M87 Black Hole Mass from Gas-dynamical Models of Space Telescope Imaging Spectrograph Observations. *ApJ*, 770:86, June 2013.
13. J. M. Bardeen. Timelike and null geodesics in the Kerr metric. In C. Dewitt and B. S. Dewitt, editors, *Black Holes*, pages 215–239, 1973.
14. V. Bozza. Gravitational lensing by black holes. *General Relativity and Gravitation*, 42:2269–2300, September 2010.
15. T. Johannsen and D. Psaltis. Testing the no-hair theorem with observations of black holes in the electromagnetic spectrum. *Advances in Space Research*, 47:528–532, February 2011.
16. T. Lacroix, M. Karami, A. E. Broderick, J. Silk, and C. Boehm. A unique probe of dark matter in the core of M87 with the Event Horizon Telescope. *ArXiv e-prints*, November 2016.
17. A. E. Broderick. Radiative transfer along rays in curved space-times. *MNRAS*, 366:L10–L12, February 2006.
18. A. E. Broderick and A. Loeb. Frequency-dependent Shift in the Image Centroid of the Black Hole at the Galactic Center as a Test of General Relativity. *ApJL*, 636:L109–L112, January 2006a.
19. A. E. Broderick and A. Loeb. Imaging optically-thin hotspots near the black hole horizon of Sgr A* at radio and near-infrared wavelengths. *MNRAS*, 367:905–916, April 2006b.
20. S. S. Doeleman, V. L. Fish, D. E. Schenck, et al. Jet-Launching Structure Resolved Near the Supermassive Black Hole in M87. *Science*, 338:355, October 2012.
21. K. Akiyama, R.-S. Lu, V. L. Fish, et al. 230 GHz VLBI Observations of M87: Event-horizon-scale Structure during an Enhanced Very-high-energy γ-Ray State in 2012. *ApJ*, 807:150, July 2015.
22. T. Johannsen and D. Psaltis. Testing the No-hair Theorem with Observations in the Electromagnetic Spectrum. II. Black Hole Images. *ApJ*, 718:446–454, July 2010.
23. T. Johannsen. Photon Rings around Kerr and Kerr-like Black Holes. *ApJ*, 777:170, November 2013.